ANSTO/E667

ANSTO/E667

AUSTRALIAN NUCLEAR SCIENCE AND TECHNOLOGY ORGANISATION

LUCAS HEIGHTS RESEARCH LABORATORIES

ANALYSIS OF MAGNETIC FIELD DATA FROM ROTAMAK VI

by

P.A. WATTERSON

NOVEMBER 1987

ISBN 0 642 59873 8

AUSTRALIAN NUCLEAR SCIENCE
AND TECHNOLOGY ORGANISATION

LUCAS HEIGHTS RESEARCH LABORATORIES

ANALYSIS OF MAGNETIC FIELD DATA FROM ROTAMAK VI

by

P. A. WATTERSON

ABSTRACT

Magnetic field data from an array of points within the Rotamak VI at the Flinders University of South Australia are analysed using a new algorithm to integrate the experimentally measured gradient of a function of two variables. Evaluation of the poloidal flux function, using both components of the magnetic field, reveals two closed flux regions, one inside and one outside the radius of the rotating magnetic field (RMF) coils. The smoothed toroidal current density features a small region of reversed current outside the RMF coils. Plasma pressure is evaluated assuming pressure balance.

National Library of Australia card number and ISBN 0 642 59873 8

The following descriptors have been selected from the INIS Thesaurus to describe the subject content of this report for information retrieval purposes. For further details please refer to IAEA-INIS-12 (INIS: Manual for Indexing) and IAEA-INIS-13 (INIS: Thesaurus) published in Vienna by the International Atomic Energy Agency.

EXPERIMENTAL DATA; ELECTRIC CURRENTS; MAGNET COILS; MAGNETIC FIELDS; MAGNETIC FLUX; PLASMA; PLASMA PRESSURE; ROTATION; ROTAMAK DEVICES

EDITORIAL NOTE

The Australian Nuclear Science and Technology Organisation (ANSTO) replaced the Australian Atomic Energy Commission (AAEC) on 27 April 1987. Reports issued after April 1987 have the prefix ANSTO with no change of the symbol (E, M, S or C) or numbering sequence.

CONTENTS

1. INTRODUCTION

In April 1986, researchers at the Flinders University of South Australia requested assistance in analysing data from the Rotamak VI experiment. This rotamak has a cylindrical, stainless steel vacuum vessel (diameter 75 cm, length 50 cm) with straight, internal rotating magnetic field (RMF) coils (at radius 15 cm) and a vertical field provided by a pair of coils of small diameter (28 cm) compared to their separation (59 cm) (see Kirolous [1986] for further details). Kirolous had measured the time-averaged magnetic field components B_r and B_z (referring to cylindrical co-ordinates (r,ϕ,z)) on an array of equispaced points in the r-z plane (80 positions to cover $0.5\text{ cm} \le r \le 40\text{ cm}$, and 33 positions to cover $|z| \le 20$ cm). In this report, the field-line topology, toroidal current density and plasma pressure are deduced from the data taken 20 ms into the discharge.

The topology of the field is best displayed by a contour plot of the poloidal flux function Ψ satisfying

$$\frac{\partial \Psi}{\partial r} = 2\pi r B_z \quad , \text{ and} \tag{1}$$

$$\frac{\partial \Psi}{\partial z} = -2\pi r B_r \quad , \tag{2}$$

the field being axisymmetric. Integrating **equation 1** from $\Psi = 0$ on $r = 0$ gives a formula based on B_z alone,

$$\Psi(r,z) = 2\pi \int_0^r B_z(r', z) r' dr' \tag{3}$$

which, when applied to the data, produces **figure 1a.** Unfortunately, systematic errors (up to 20 per cent) along rows (at constant z) of the data result in random steps in Ψ with z which at large r are bigger than the features in Ψ that are sought.

To improve on this evaluation of Ψ, an algorithm was developed to integrate the gradient of a function of two variables

$$\nabla f = \mathbf{V} \quad , \tag{4}$$

where the experimentally measured vector field $\mathbf{V}$ is supposed to be irrotational ($\nabla \wedge \mathbf{V} = 0$). The algorithm, described in **section 2** below, blends both components of $\mathbf{V}$ *via* a least squares minimisation, with weighting factors to reduce the significance of one or other component of the data or regions of the data which are considered less reliable. **Section 3** presents the smooth Ψ obtained when the algorithm is applied to $\nabla\Psi$ given by **equations 1-2.**

Section 4 compares the toroidal current density J_ϕ calculated by two methods: first-order differencing of the original magnetic field data, and second-order differencing of the calculated Ψ. The former is found to be less noisy and, after smoothing by a cubic spline method, a clear contour plot of J_ϕ is obtained.

In **section 5**, the integration algorithm is used a second time to evaluate the plasma pressure P from the pressure balance equation

$$\nabla P = \mathbf{J} \wedge \mathbf{B} \quad . \tag{5}$$

In this case the measured $\mathbf{J} \wedge \mathbf{B}$ may be only approximately irrotational owing to other physical effects neglected in **equation 5**, in addition to inaccuracies in the experimental measurement.

Kirolous [1986] analysed the data by first fitting B_r and B_z with two-dimensional polynomial expressions, antisymmetric and symmetric, respectively, about $z = 0$ and constrained by $\nabla \cdot \mathbf{B} = 0$. Thus he determined a Ψ of form

$$\Psi = \sum_{i=0}^{n_1} \sum_{j=0}^{n_2} C_{ij} r^{2i+2} z^{2j} \quad . \tag{6}$$

One drawback of this method is that even if the experimental errors were very small and there was little uncertainty in Ψ, the restriction to **form 6** with given n_1 and n_2 means that only an approximation to Ψ would be found. Kirolous used $n_1 = 8$ and $n_2 = 4$ which may have been too low to detect all the structure present in the data - in particular, it would appear from his **figures 6.25** and **6.26** that the maxima of both B_z and B_r were always underestimated by the fitting procedure. The algorithm presented here does not have the above defect as it integrates $\nabla\Psi$ without imposing a form or symmetry upon Ψ.

2. AN ALGORITHM TO INTEGRATE THE GRADIENT OF A FUNCTION OF TWO VARIABLES

This section presents an algorithm to integrate the two-dimensional gradient

$$\frac{\partial f}{\partial r} = V_r \ , \tag{7}$$

$$\frac{\partial f}{\partial z} = V_z \ , \tag{8}$$

given V_r and V_z on a grid of equispaced points. The algorithm is intended for use when **V** is supposed to be irrotational (*i.e.* $\partial V_r/\partial z - \partial V_z/\partial r = 0$) but is only approximately so, due, for example, to errors in experimental measurement. We label the (r,z) grid positions by (i,j) for $i = 1,2,...n_r$ and $j = 1,2,...n_z$, and denote the grid spacings by Δ_r and Δ_z. By integrating **equation 8** we can obtain f (up to an arbitrary additive constant) for $i = 1$. In the applications of the algorithm in this work, $V_z = 0$ on $i = 1$ (corresponding to $r = 0$) and f is set to an arbitrary constant on $i = 1$ (for Ψ this constant is 0). From the following algorithm f is obtained in columns (of constant r), from $i = 2$ to n_r.

Suppose we have f(i,j) for a given i and $j = 1,2,...n_z$, and wish to determine $X(j) = f(i+1,j)$ for $j = 1,2,...n_z$. According to **equation 7** the difference $X(j) - f(i,j)$ should be set equal to

$$D_r(j) = \Delta_r\Big[V_r(i,j) + V_r(i+1,j)\Big]/2 \ , \tag{9}$$

but for **equation 8** to be satisfied, the difference X(j+1) - X(j) should equal

$$D_z(j) = \Delta_z\Big[V_z(i+1,j) + V_z(i+1,j+1)\Big]/2 \ . \tag{10}$$

The problem is clearly overconstrained and some errors must be accepted:

$$E_r(j) = (X(j) - f(i,j)) - D_r(j) \ , \ j = 1,2,...n_z \ , \tag{11}$$

$$E_z(j) = (X(j+1) - X(j)) - D_z(j) \ , \ j = 1,2,...n_z-1 \ . \tag{12}$$

The parameter α is introduced to weight the V_r or V_z data and the vectors W_r and W_z to weight the rows of data; **X** is determined by minimising

$$F(\mathbf{X}) = \alpha \sum_{j=1}^{n_z} W_r(j)\left[\frac{E_r(j)}{\Delta_r}\right]^2 + (1-\alpha)\sum_{j=1}^{n_z-1} W_z(j)\left[\frac{E_z(j)}{\Delta_z}\right]^2 \ . \tag{13}$$

Note that the errors have been divided by the corresponding step length, so that if a step length is larger in one direction, correspondingly larger errors are tolerated in that direction. If the V_r and V_z data are regarded as equally reliable, then $\alpha = 1/2$ should be adopted.

It is straightforward to show (by differentiating with respect to X(j)) that F is at a minimum when

$$\begin{aligned} &-(1-\beta)W_z(j-1)X(j-1) + \Big[\beta W_r(j) + (1-\beta)(W_z(j-1) + W_z(j))\Big]X(j) - (1-\beta)W_z(j)X(j+1) \\ &= \beta W_r(j)(f(i,j) + D_r(j)) + (1-\beta)\Big[-W_z(j)D_z(j) + W_z(j-1)D_z(j-1)\Big] \ , \quad \text{for } j = 1,2,...n_z \ , \end{aligned} \tag{14}$$

where

$$\beta = \Big[1 + (1-\alpha)\,\Delta_r^2/\alpha\Delta_z^2\Big]^{-1} \ , \tag{15}$$

and for $j = 1$ and n_z, terms involving $W_z(0)$ and $W_z(n_z)$ are to be neglected. In general, this tridiagonal system of linear equations can be easily solved for **X**. For $\alpha = 1$ the solution is

$$X(j) = f(i,j) + D_r(j) \ , \ j = 1,2,...n_z \ ; \tag{16}$$

$F = 0$, and only the V_r data are utilised. For $\alpha = 0$, the system may be shown to be equivalent to

$$X(j+1) - X(j) = D_z(j) \ , \ j = 1,2,...n_z-1 \ , \tag{17}$$

and is singular, with non-unique solution. Thus, if more weight is to be given to the V_z data, α should be made a small but non-zero value.

3. EVALUATION OF Ψ

The algorithm described above was used to obtain Ψ for various values of α, with no z-dependent weighting (*i.e.* with W_r and W_z equal 1). The Ψ calculated for $\alpha = 1$, *i.e.* from the B_z field alone, is given in **figure 1a**. Using the same contour intervals, **figures 1b-d** give the Ψ calculated for $\alpha = 0.75$, $\alpha = 0.5$ and $\alpha = 0.02$. The incorporation of the B_r data in the calculation is seen to produce a smoothing of the Ψ contours. Whereas for $\alpha = 1$ only an inner region of closed flux contours can be reliably discerned, from the other plots it is clear that there is also an outer closed flux contour region separated from the first by a band of open field lines and an X-type neutral point. There is also some evidence that the outer closed region divides through $z \approx 0$ into two small closed regions - the lower region is prominent in the $\alpha = 0.75$ and $\alpha = 0.5$ plots, and the upper region is brought out by the B_r data in the $\alpha = 0.02$ plot. More accurate field measurements are needed to confirm this result.

We regard the Ψ calculated for $\alpha = 0.5$ (see **figure 1c**) as optimal, blending the B_r and B_z data equally. **Figures 2** and **3** compare the measured field with that deduced from this calculated Ψ, at various fixed r and z. It would seem that the B_z data have actually been better fitted than the B_r data. Note in particular how B_r has been reduced in magnitude over much of the region $0 < r \leq 20$ cm, -20 cm $\leq z \leq 0$ as a means of ensuring $\nabla \cdot \mathbf{B} = 0$. The zero offset of the measured B_r at $r = 0$ for $z = 0$, -5 cm and -10 cm (see **figure 3**) indicates that there the B_r data is unreliable. If the data were symmetrised about $z = 0$ the fit for B_r would by chance be improved, for example the calculated maximum B_r amplitude is high at $z = 5$ cm but low at $z = -5$ cm (see **figures 3b** and **c**). However, we choose to analyse the original data, rather than reduce apparent errors by symmetrisation.

4. EVALUATION OF J_ϕ

Two finite-difference methods have been used to calculate J_ϕ. The more straightforward method evaluates

$$J_\phi = \frac{1}{\mu_0}\left[\frac{\partial B_r}{\partial z} - \frac{\partial B_z}{\partial r}\right] , \tag{18}$$

using centred differencing on the raw B_r and B_z data. The resulting J_ϕ is shown in **figure 4** as a contour plot (with negative contours dashed and $J_\phi = 0$ included as a full line) and on $z = 0$. The second method, giving J_ϕ for each value of α, takes the Ψ given by the algorithm of **section 2**, and evaluates

$$J_\phi = -\frac{1}{2\pi\mu_0}\left[\frac{1}{r}\frac{\partial^2\Psi}{\partial z^2} + \frac{\partial}{\partial r}\left[\frac{1}{r}\frac{\partial\Psi}{\partial r}\right]\right] , \tag{19}$$

using three-point difference expressions. The J_ϕ derived for $\alpha = 0.5$ is shown in **figure 5**. Although the smoothing effected in the evaluation of Ψ was expected to produce a smoother J_ϕ by **equation 19**, this J_ϕ is, in fact, slightly noisier. In both cases, the large J_ϕ alternating in sign with z at large $|z|$ is probably spurious. In particular, the J_ϕ on the domain boundary was found by linear extrapolation and should be ignored.

To make the features of J_ϕ more apparent, a program was written to smooth the array of J_ϕ values. First, each column of J_ϕ values (at fixed r) was separately smoothed; then, adopting the new smoothed J_ϕ values, each row was separately smoothed. The smoothing was performed by the IMSL procedure ICSSCU, which for data f(i) at x(i), i=1,2...N, obtains a cubic spline S with the smallest $\int [S''(x)]^2 dx$, while satisfying $\sum_{i=1}^{N}\left[[S(x(i)) - f(i)]/W(i)\right]^2 \leq E$ for specified constant E and weights W(i).

Figure 6a gives a contour plot of the smoothed J_ϕ calculated from B_r and B_z (*cf.* **figure 4a**) using smoothing parameter $E = 8$ and weights $W(j) = 1+4|z(j)/z(n_z)|^2$ for the z-direction, and $E = 20$ and $W(i) = 1$ for the r-direction. The region of highest J_ϕ lies within $0 < r \leq 15$ cm, $|z| \leq 7.5$ cm with maximum value $J_\phi \approx 2.5 \times 10^4$ A m^{-2} at $r = 10$ cm, $z = 0$. Within the region 15 cm $\leq r \leq 25$ cm, $|z| \leq 5$ cm, J_ϕ is negative with largest magnitude $J_\phi \approx -5 \times 10^3$ A m^{-2} at $r = 20$ cm, $z = 0$. This small negative J_ϕ region is flanked by regions of positive J_ϕ with maximum value $J_\phi \approx 1 \times 10^4$ A m^{-2} at $r \approx 25$ cm, $z \approx \pm 11$ cm. The efficacy of the smoothing may be gauged from **figures 6b** and **c**, showing J_ϕ on $z = 0$ and $r = 10$ cm. The fit is generally good except that the maximum J_ϕ seems to have been underestimated.

The total toroidal current, found by integrating the raw B_r and B_z data around the perimeter of the measurement domain, was

$$I_\phi = \frac{1}{\mu_0} \int \mathbf{B}.\mathbf{dl} = 625 \text{ A} \quad . \tag{20}$$

The toroidal current over the domain $0 \le r \le 15$ cm was 310 A, so the total current was almost equally divided between the regions inside and outside the RMF coils.

5. EVALUATION OF P

The plasma pressure P is evaluated by assuming that pressure balance (**equation 5**) holds and integrating

$$\frac{\partial P}{\partial r} = J_\phi B_z \quad , \tag{21}$$

$$\frac{\partial P}{\partial z} = -J_\phi B_r \quad , \tag{22}$$

using the algorithm of **section 2**. To give equal weighting to the B_r and B_z data, we choose $\alpha = 0.5$ and, because the integration involves smoothing, it is sufficient to use the unsmoothed J_ϕ derived from B_r and B_z. This J_ϕ is unreliable at large $|z|$, however, and the following weighting functions are employed:

$$W_r(j),\ j = 1,\ldots n_z = \left\{ \begin{array}{l} W_z(j-1),\ j = 2,\ldots (n_z-1)/2 \\ W_z(j),\ j = (n_z+1)/2,\ldots n_z - 1 \end{array} \right\} = \left[1 + 5 \left| \frac{z(j)}{z(n_z)} \right|^3 \right]^{-1} \quad . \tag{23}$$

(In fact we further reduced W_r by a factor of 10 and W_z by a factor of 5 at their end points, to minimise the influence of J_ϕ on the domain boundary.)

Figure 7 shows the resulting P assuming $P = 0.5$ Pa on $r = 0$, sufficient to keep $P > 0$ everywhere (except at large $|z|$). P rises to a maximum of about 0.7 Pa on the magnetic axis (at $r = 7$ cm, $z = 0$) and falls to near-zero at $r = 15$ cm, $z = 0$, where there is a well in P with depth of about 0.1 Pa. **Figure 7c** shows that outside the RMF coils P is fairly flat (provided that the effect of the unrealistically large J_ϕ at large $|z|$ is neglected).

6. DISCUSSION AND CONCLUSIONS

The principal results of this analysis are the Ψ, J_ϕ and P shown in **figures 1c, 6** and **7**. In summary, Ψ and P have been obtained by integrating $\nabla\Psi = 2\pi r \hat{\underline{\Phi}}\ \mathbf{B}$ and $\nabla P = \mathbf{J} \wedge \mathbf{B}$, using a least squares minimisation at each column of grid points (at constant r). The raw B_r and B_z and derived J_ϕ (by centred differencing) were used in the right-hand side of these expressions, and a z-dependent weighting was incorporated in the P calculation because J_ϕ was unreliable at large $|z|$. To clarify the features of J_ϕ, smoothing by a one-dimensional cubic spine method was performed, first for each column and then for each row.

Variations on the above methods could be attempted. It would be possible to reformulate the integration algorithm (**section 2**) so that the minimisation was carried out globally rather than column by column, but this would involve the solution of $n_z \times (n_r - 1)$ simultaneous equations. In the calculation of Ψ a z-dependent weighting could have been applied (as in the calculation of P), but there was no *a priori* reason to suspect the data from any z region. A two-dimensional smoothing method for J_ϕ might have been superior, the local cubic spline fitting being favoured as it imposed no functional form on the data.

Let us compare these results with those obtained by Kirolous [1986] after fitting the B_r and B_z data by two-dimensional polynomials (as described in **section 1**). His Ψ, reproduced in **figure 8a**, is much smoother than the Ψ computed by our algorithm for $\alpha = 0.5$ (**figure 1c**). Nevertheless, his Ψ has an additional, small feature, namely an additional closed flux region about $r = 22$ cm, $z = 0$, whereas in ours the outer separatrix has a simple X-type neutral point. The additional closed flux region has obviously been extracted from the B_z data as it is present in our $\alpha = 1$ and $\alpha = 0.75$ plots (**figures 1a** and **b**). Its existence seems improbable as it makes the field structure topologically more complicated.

J_ϕ of Kirolous, reproduced in **figure 8b**, shows broadly similar features to our smoothed J_ϕ (**figure 6a**). They differ slightly in that in his calculation the negative J_ϕ region extends to within the RMF coils. This appears doubtful on consideration of the unsmoothed J_ϕ (**figure 4a**).

Kirolous calculated P using his fitted variables and **equation 21**, *i.e.*

$$P = P_0 + \int_0^r J_\phi (r',z)\, B_z (r',z) dr' \quad , \tag{24}$$

to obtain the P reproduced in **figure 8c**. The resulting difference between the maximum and minimum P on $z = 0$ was 0.44 Pa, which is markedly different from our value (0.63 Pa). If $J_\phi B_z$ is integrated on $z = 0$ using the 'raw values' (*i.e.* the measured B_z and J_ϕ given by **equation 18**) the result is 0.61 Pa, supporting our value. Actually his P has a minimum, not on $z = 0$ but in troughs at $z \approx \pm 7$ cm, and the difference between the maximum P and this global minimum is roughly 0.6 Pa. The value he adopted for P_0, namely 0.3 Pa, was not, in fact, sufficient to keep $P > 0$ in these troughs.

The inadequacy of using **equation 21** alone to calculate P, neglecting **equation 22**, is evident on considering the profile of the resulting P at a fixed large r (≈ 30 cm). Moving to positive z from $z = 0$, his P falls into a deep trough then rises to a maximum near the positive J_ϕ maximum (at around $z = 13$ cm). However, on this whole interval his J_ϕ and B_r are positives so if **equation 22** were employed P should fall monotonically from a maximum on $z = 0$. This inconsistency can be directly attributed to the fact that for his fitted fields $\nabla \wedge (\mathbf{J} \wedge \mathbf{B})$ was approximately zero (*i.e.* small relative to the magnitude of its two components) only over the region $0 \leq r \leq 15$ cm, $|z| \leq 7.5$ cm (see his **figure 7.1**).

In our results, too, there are indications that pressure balance could only have held (approximately) within the inner region of closed field lines. There, the P and Ψ contours do roughly coincide. Elsewhere, comparison of **figures 1c** and **6a** shows that J_ϕ / r is not constant on each flux contour, as would be implied by pressure balance. In particular, the region of negative J_ϕ does not extend along the field lines passing through it. Also J_ϕ does not increase with r along the field lines passing through the side lobes of positive J_ϕ (at $r \approx 25$ cm, $z \approx \pm 10$ cm). These features indicate that pressure balance does not apply outside the RMF coils.

7. ACKNOWLEDGEMENTS

Much credit is due to H.A. Kirolous for the experimental results described in this work. The author would also like to thank Professor I.R. Jones for bringing the problem to his attention and D. Brotherton-Ratcliffe for organising the computer link by which the data were transferred. In addition, G.A. Collins and I.J. Donnelly gave valuable suggestions which improved this report.

8. REFERENCE

Kirolous, H.A.M. [1986] - Theoretical and experimental studies of the magnetic fields of a rotamak discharge. PhD Thesis, Flinders University of South Australia.

NOTES

(a)

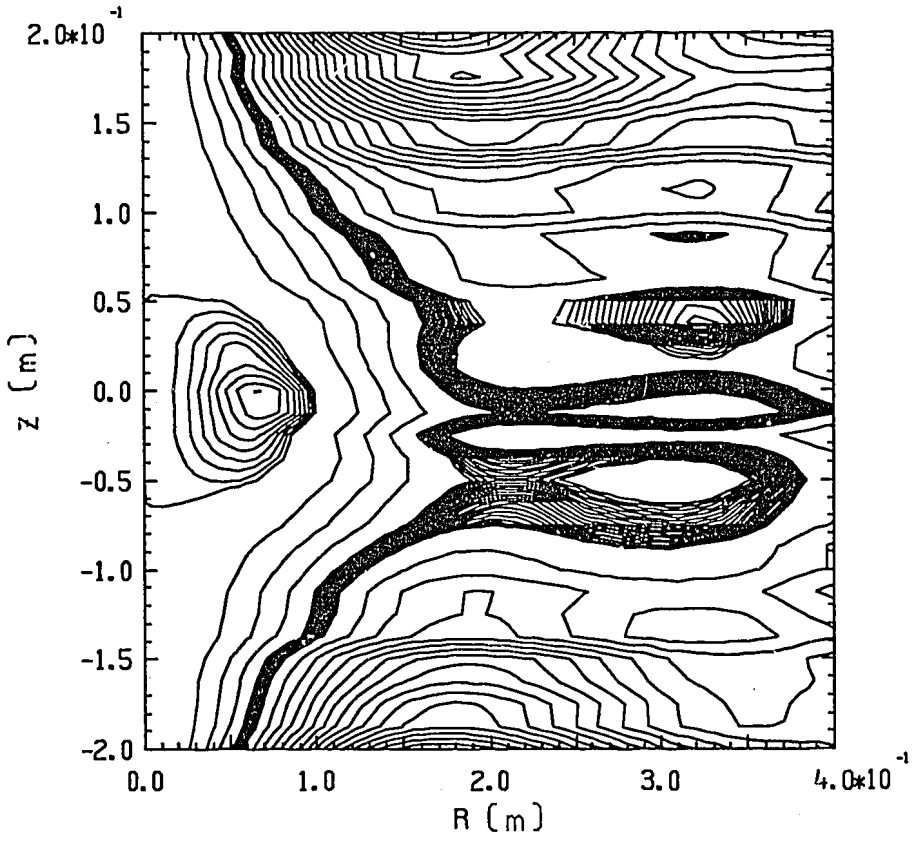

(b)

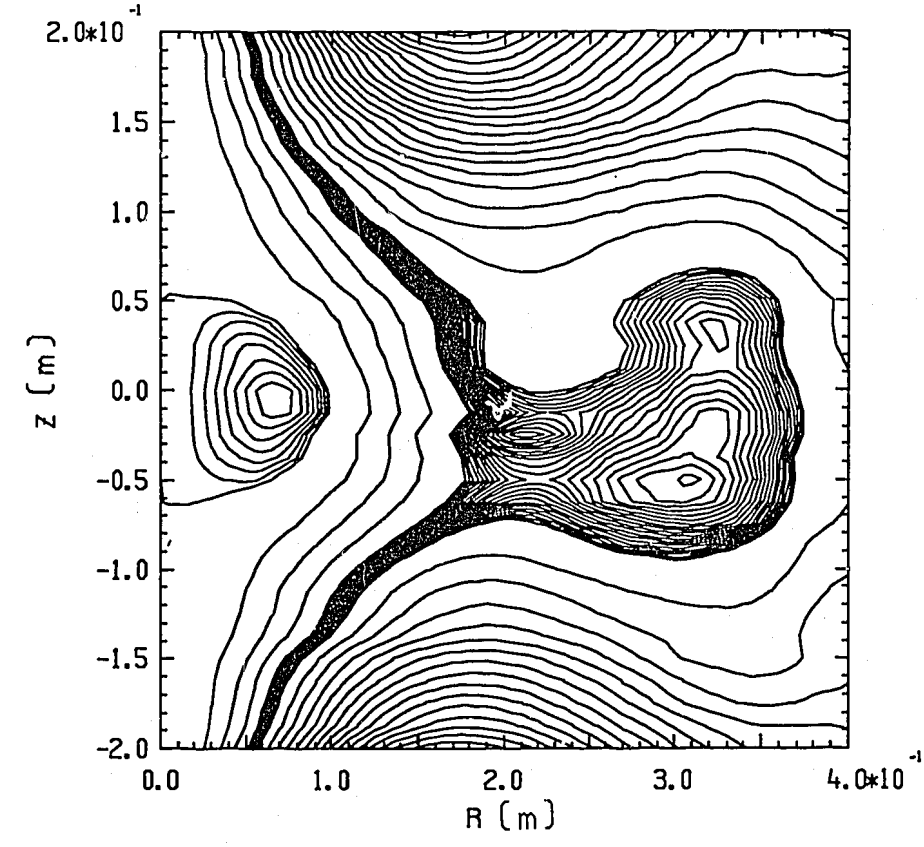

Figure 1 Ψ computed for: (a) $\alpha = 1$ (*i.e.* from B_z data alone); (b) $\alpha = 0.75$; (c) $\alpha = 0.5$; (d) $\alpha = 0.02$. Contour intervals: 1×10^{-5} Wb on $\Psi \leq -5 \times 10^{-5}$ Wb and -4×10^{-5} Wb $\leq \Psi \leq 0$; and 5×10^{-7} Wb on -5×10^{-5} Wb $\leq \Psi - 4 \times 10^{-5}$ Wb and $0 \leq \Psi$.

(Continued)

(c)

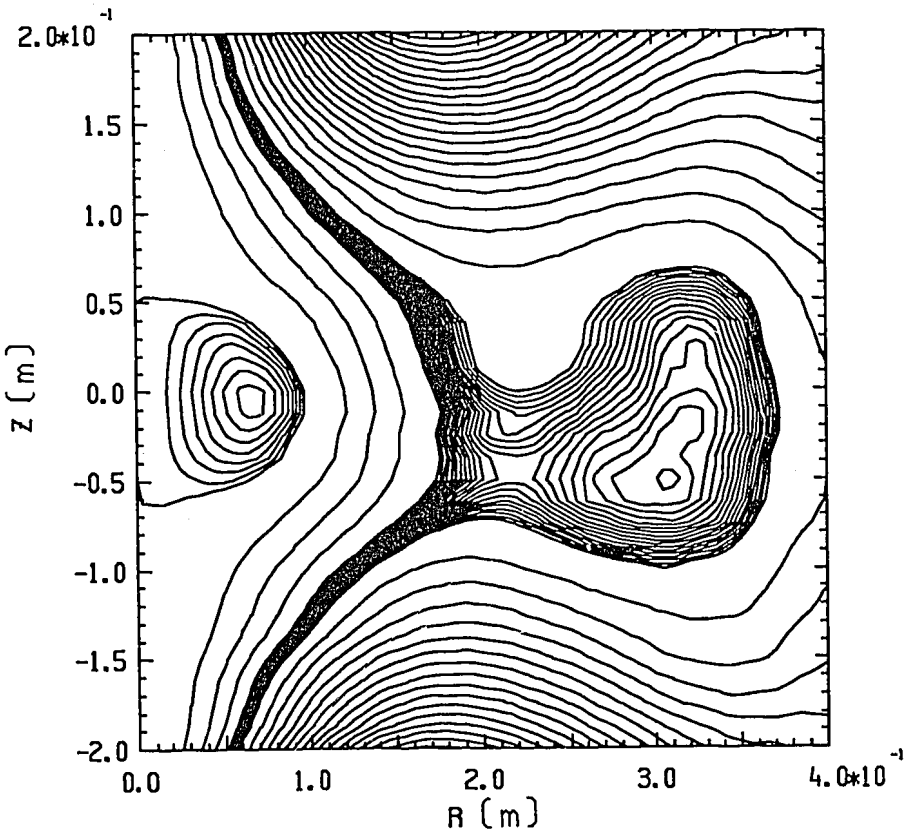
2.0*10^-1
1.5
1.0
0.5
0.0
-0.5
-1.0
-1.5
-2.0
Z (m)
0.0
1.0
2.0
3.0
4.0*10^-1
R (m)

(d)

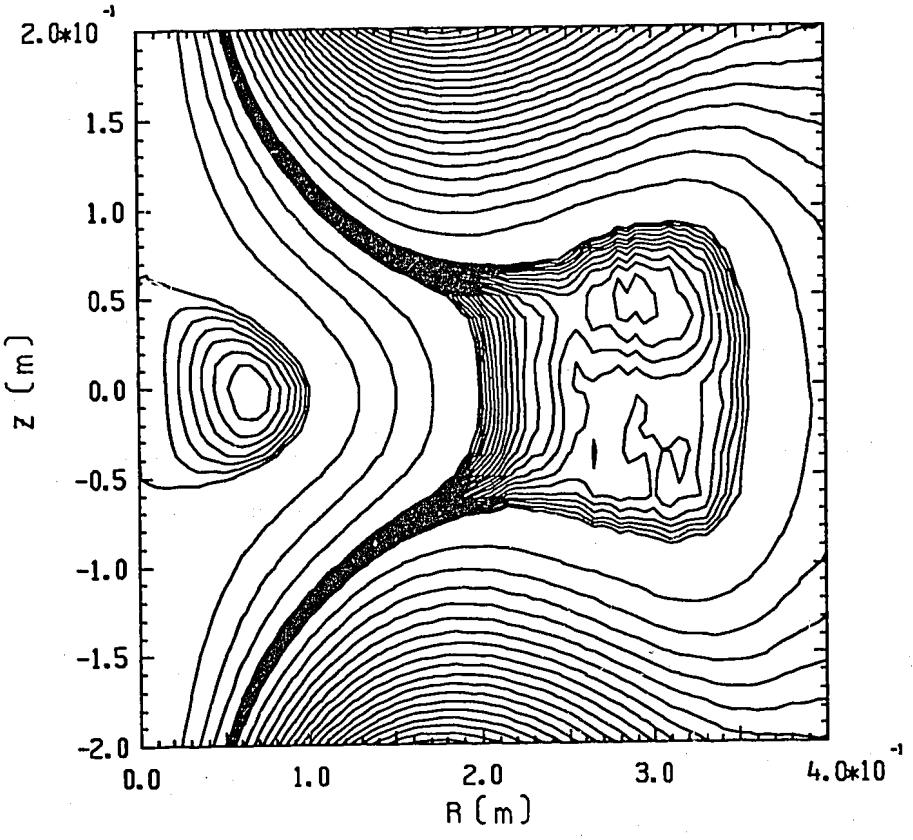
2.0*10^-1
1.5
1.0
0.5
0.0
-0.5
-1.0
-1.5
-2.0
Z (m)
0.0
1.0
2.0
3.0
4.0*10^-1
R (m)

Figure 1

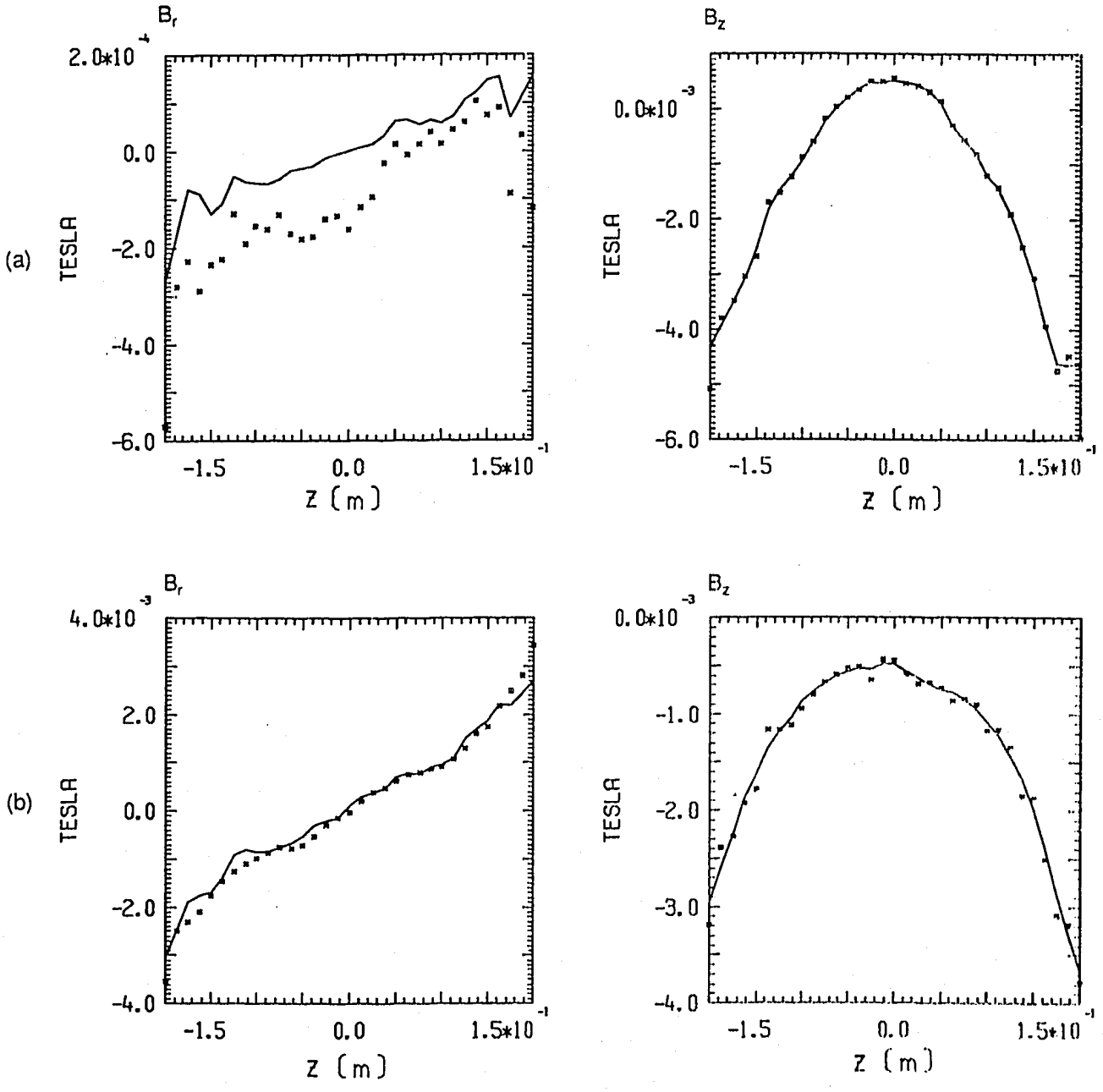

Figure 2 Comparison of B_r and B_z deduced from Ψ (for $\alpha = 0.5$) with experimental values (dotted) at (a) r = 0.5 cm; (b) r = 10 cm; (c) r = 20 cm; and (d) r = 30 cm.

(Continued)

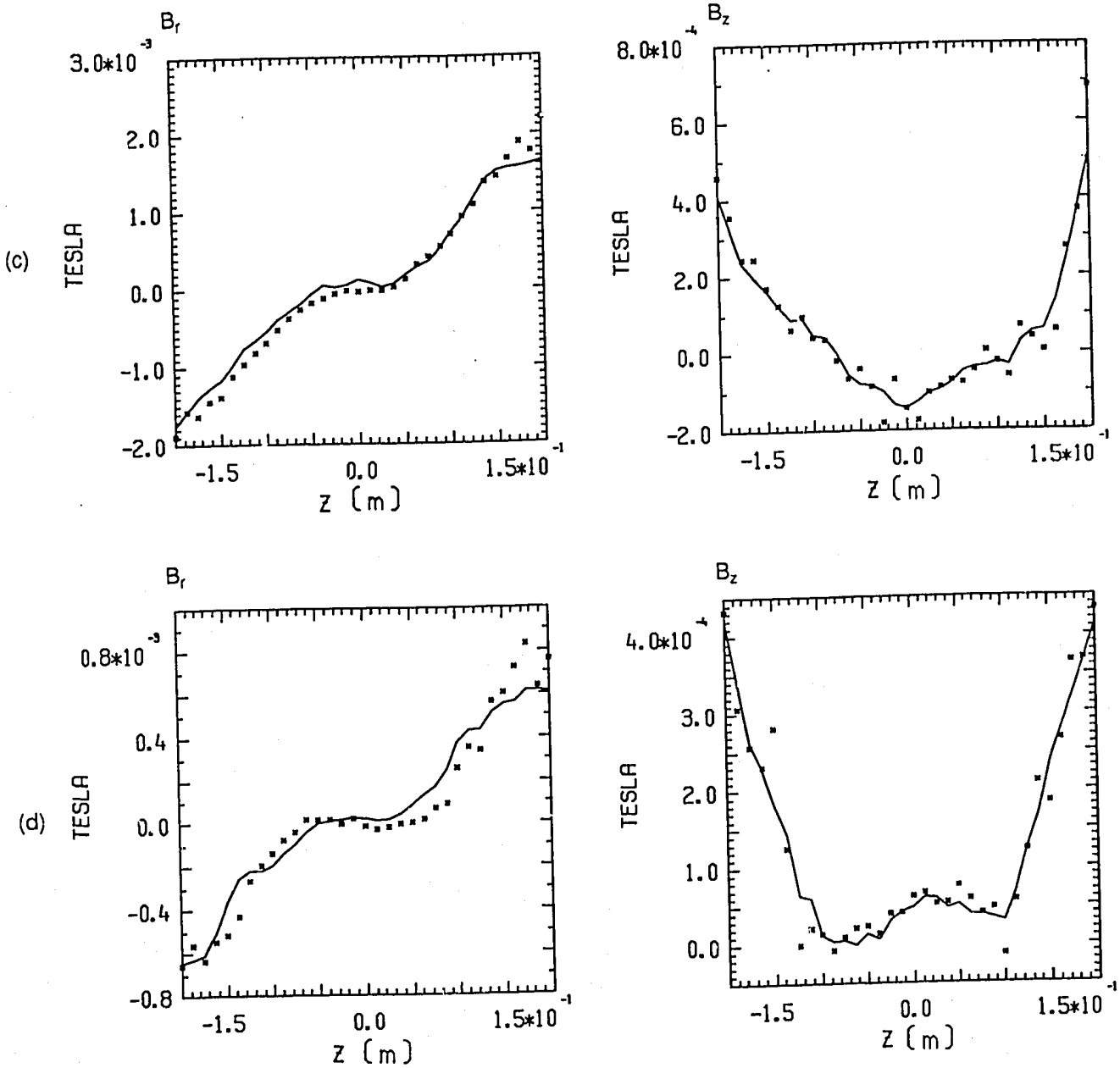
(c)
B_r
$3.0*10^{-3}$
2.0
1.0
0.0
-1.0
-2.0
TESLA
-1.5
0.0
$1.5*10^{-1}$
Z (m)
B_z
$8.0*10^{-4}$
6.0
4.0
2.0
0.0
-2.0
TESLA
-1.5
0.0
$1.5*10^{-1}$
Z (m)
(d)
B_r
$0.8*10^{-3}$
0.4
0.0
-0.4
-0.8
TESLA
-1.5
0.0
$1.5*10^{-1}$
Z (m)
B_z
$4.0*10^{-4}$
3.0
2.0
1.0
0.0
TESLA
-1.5
0.0
$1.5*10^{-1}$
Z (m)

Figure 2

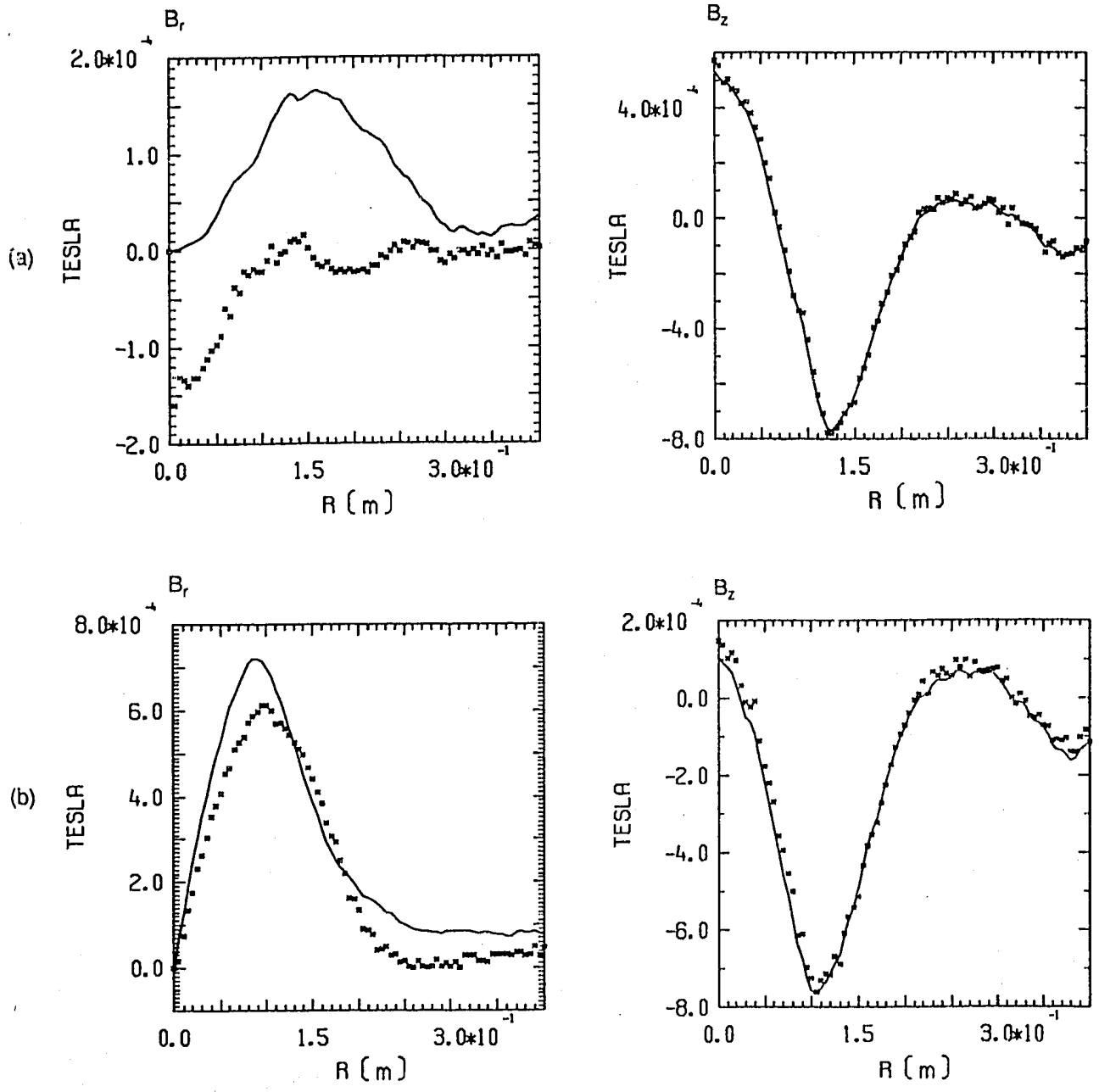

Figure 3 Comparison of B_r and B_z deduced from Ψ (for $\alpha = 0.5$) with experimental values (dotted) at (a) z = 0; (b) z = 5 cm; (c) z = -5 cm; (d) z = 10 cm; and (e) z = -10 cm.

(Continued)

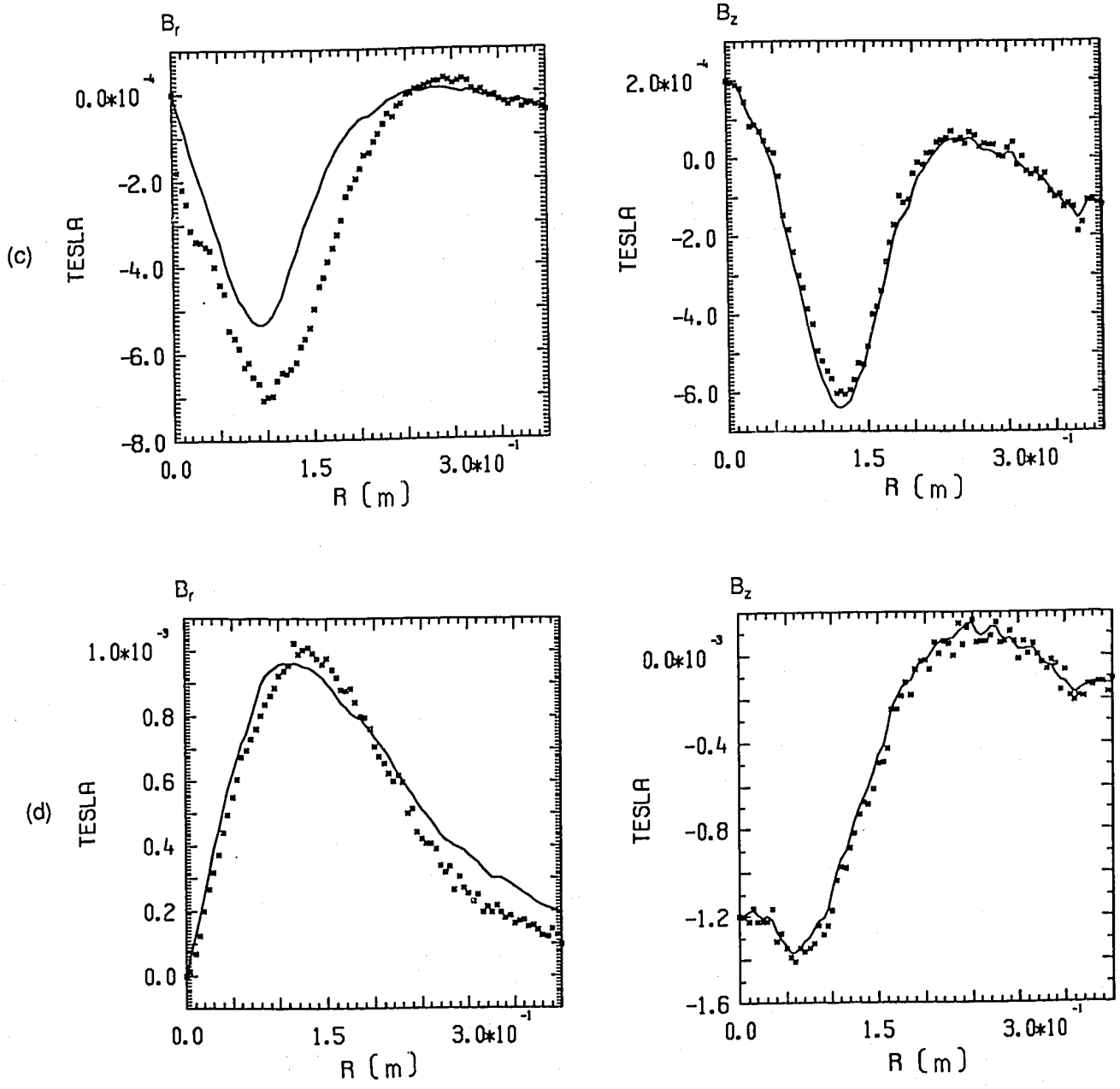

Figure 3 (Continued)

(e)

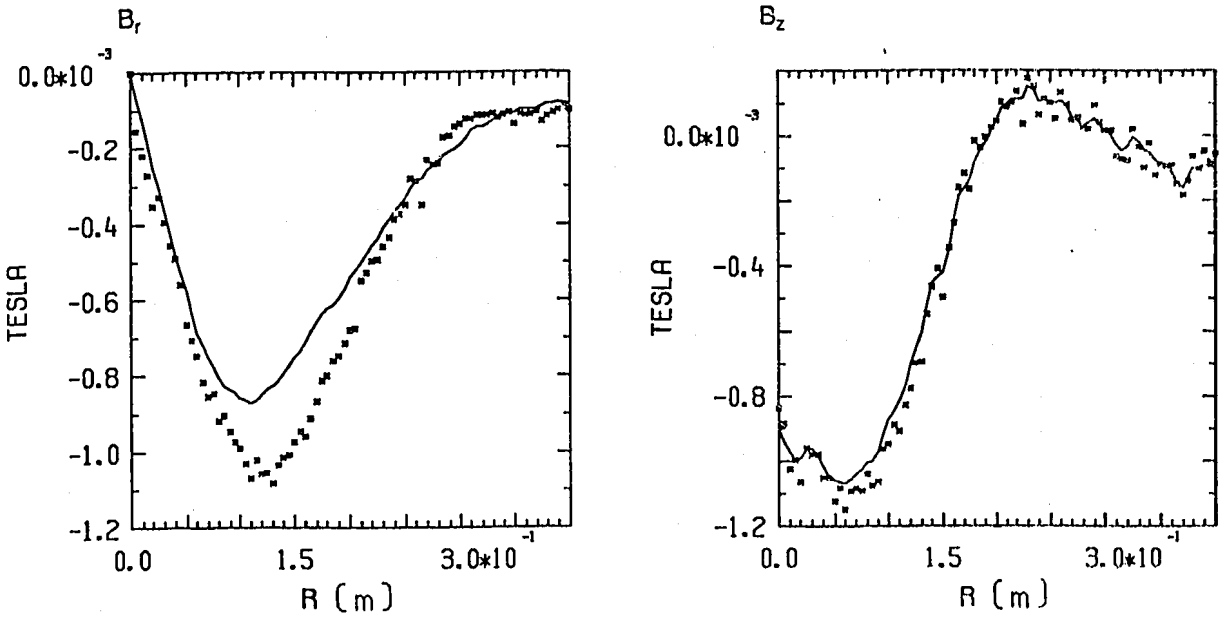

Figure 3

(a)

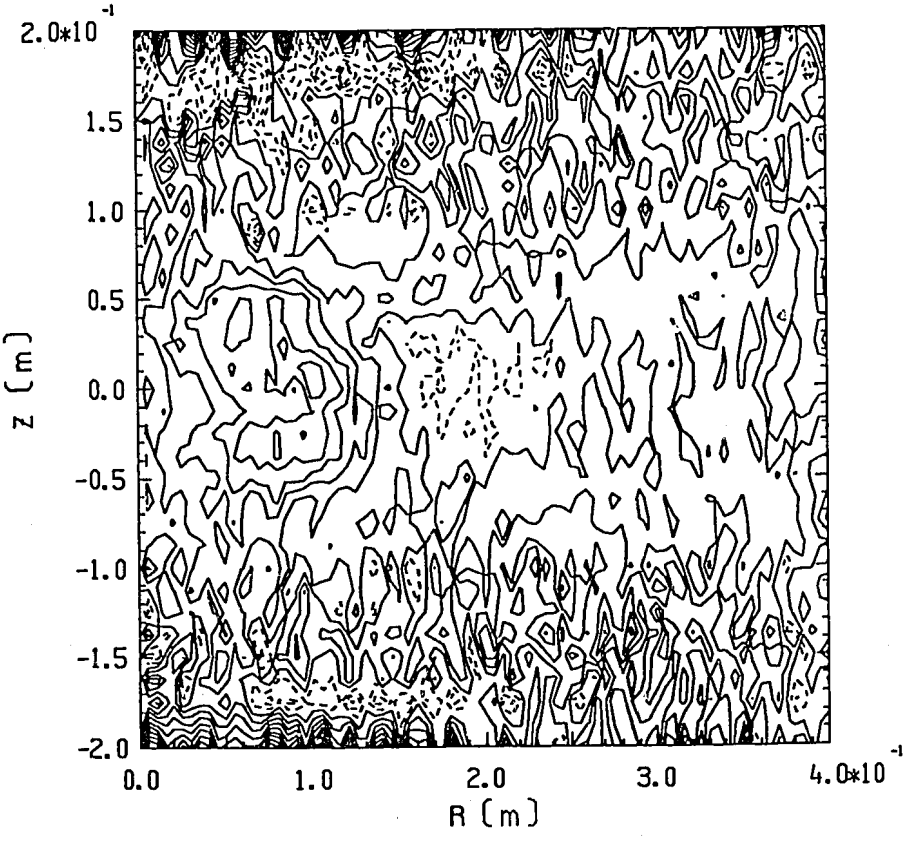

(b)

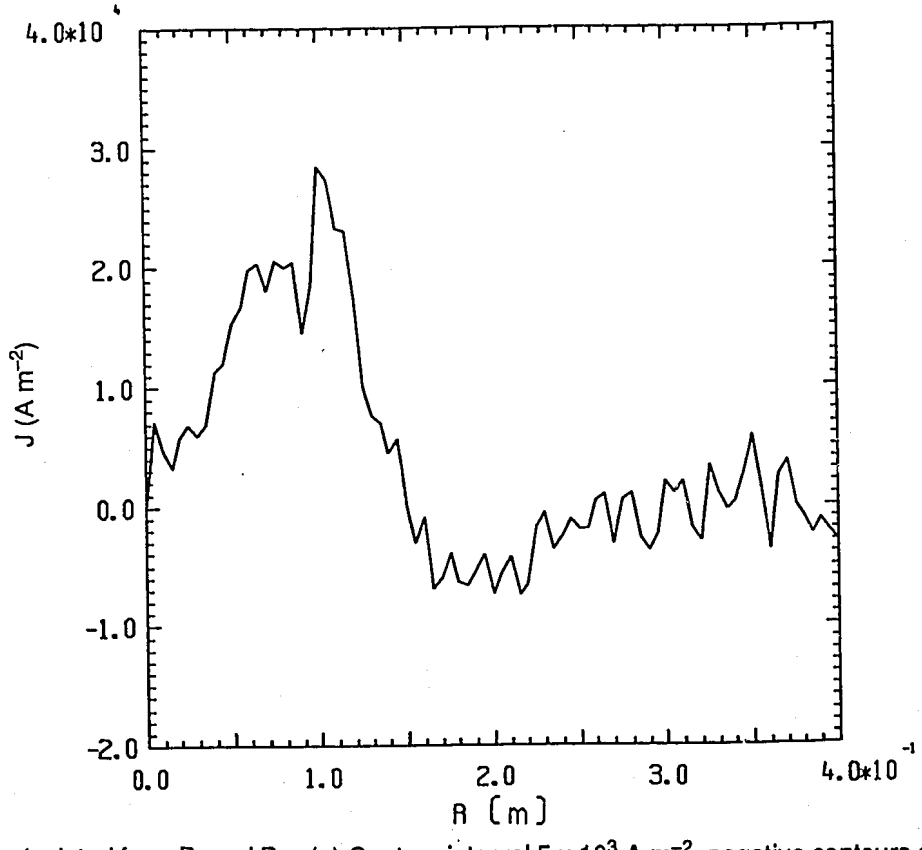

Figure 4 J_ϕ calculated from B_r and B_z. (a) Contour interval 5 x 10^3 A m^{-2}, negative contours dashed; (b) J_ϕ on z = 0.

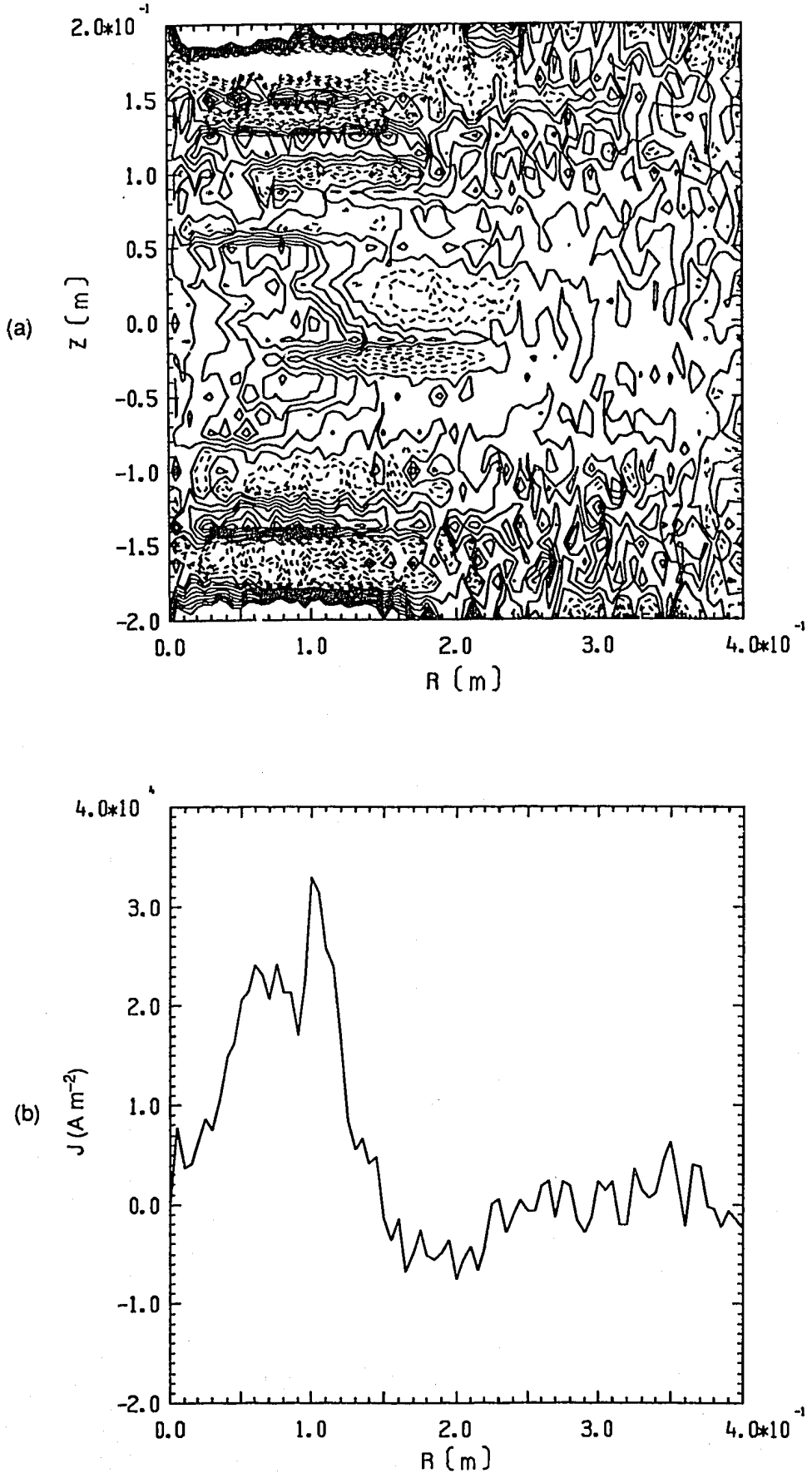

Figure 5 J_ϕ calculated from Ψ for $\alpha = 0.5$. (a) Contour interval 5×10^3 A m^{-2}, negative contours dashed; (b) J_ϕ on $z = 0$.

(a)

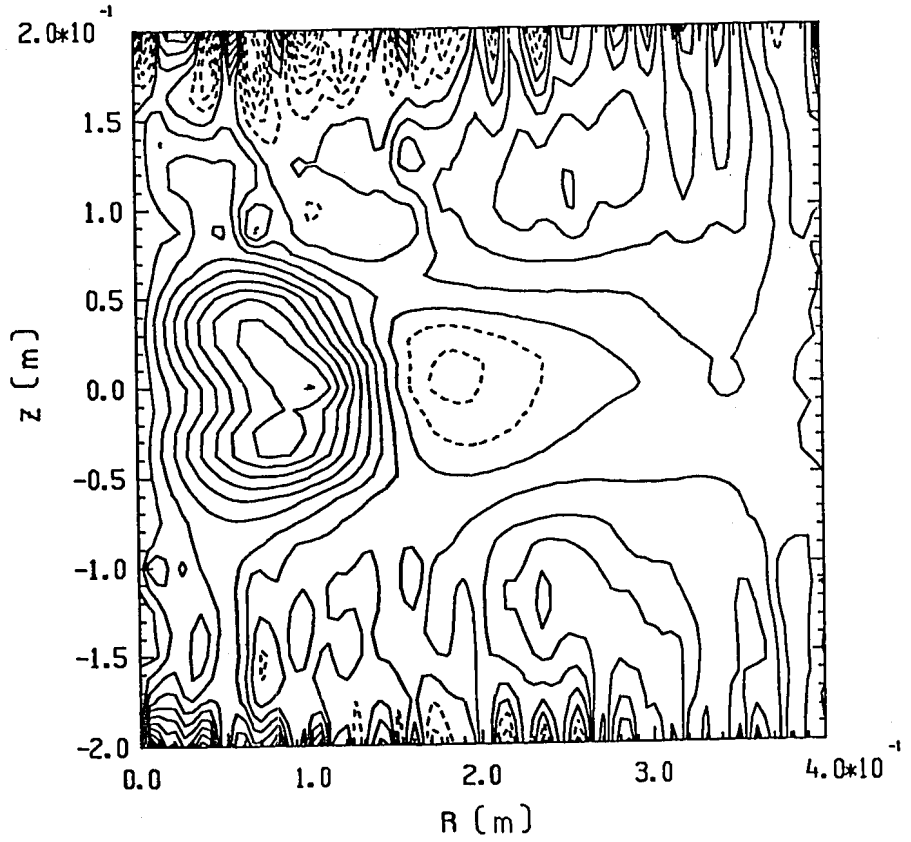

(b)

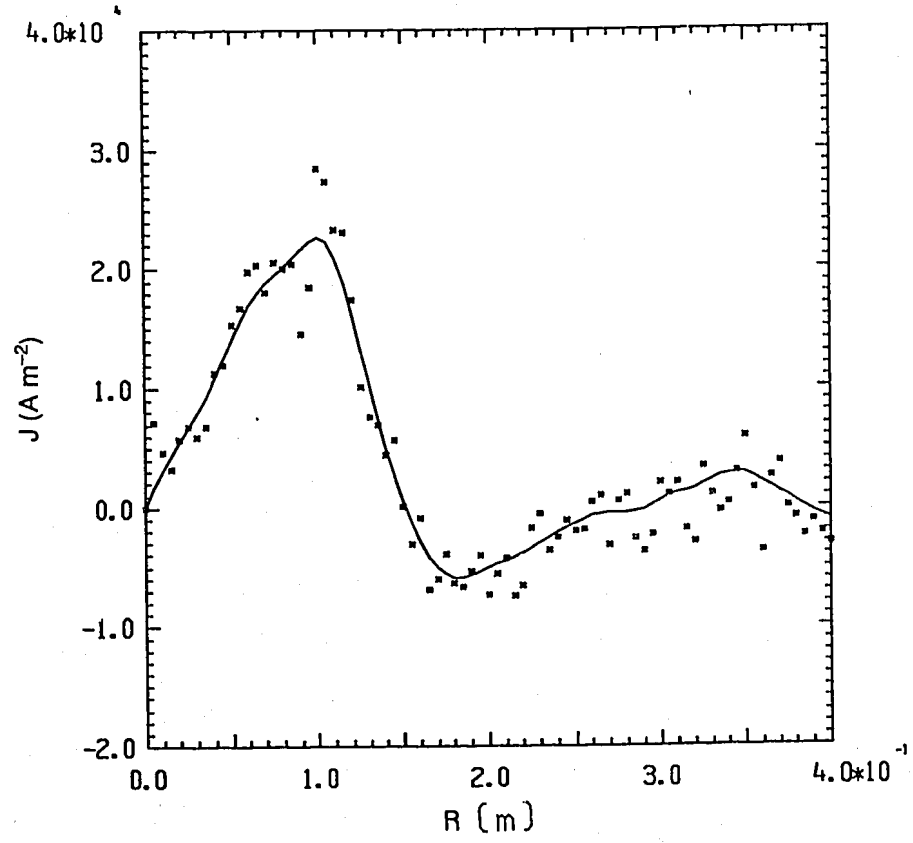

Figure 6 Smoothed J_ϕ calculated from B_r and B_z. (a) Contour interval 2.5×10^3 A m^{-2}, negative contours dashed; (b) J_ϕ on $z = 0$; (c) J_ϕ on $r = 10$ cm with unsmoothed values dotted.

(Continued)

(c)

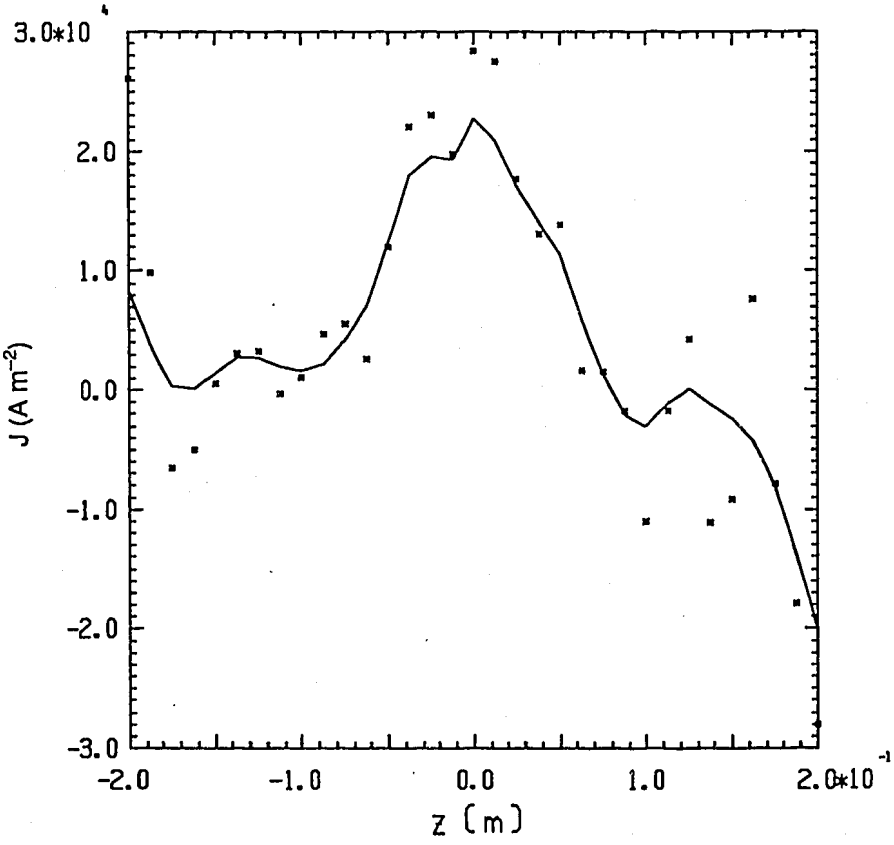

Figure 6

(a)

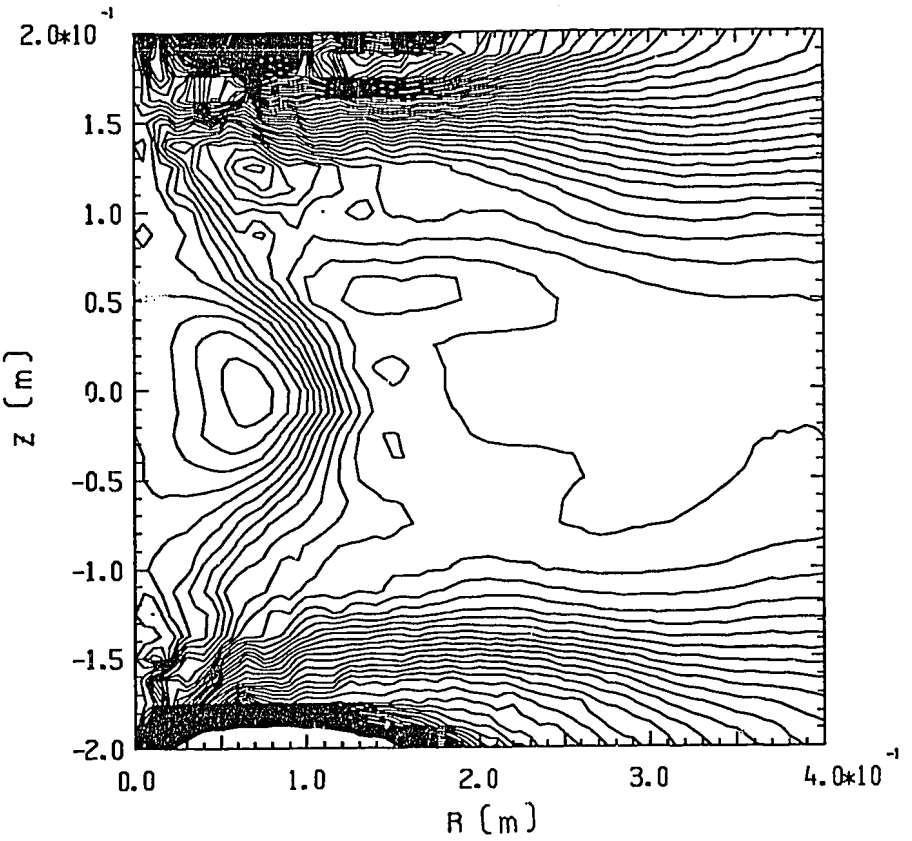

(b)

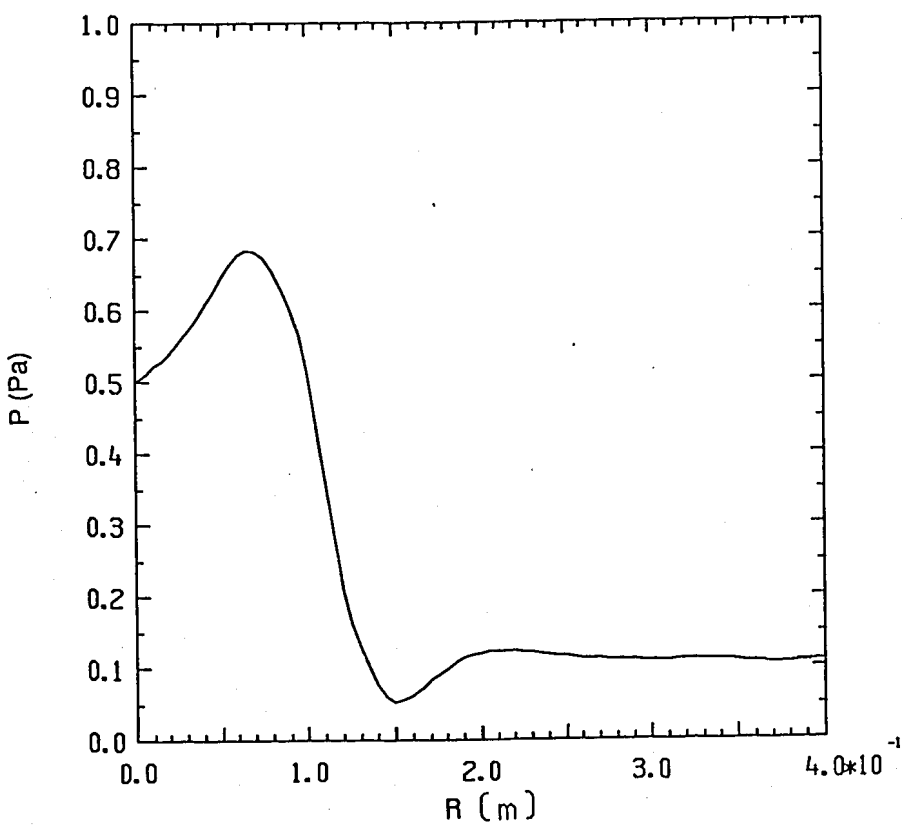

Figure 7 P (for $\alpha = 0.5$): (a) Contour interval 0.1 Pa; (b) P on $z = 0$; (c) a 3-D perspective.
(Continued)

(c)

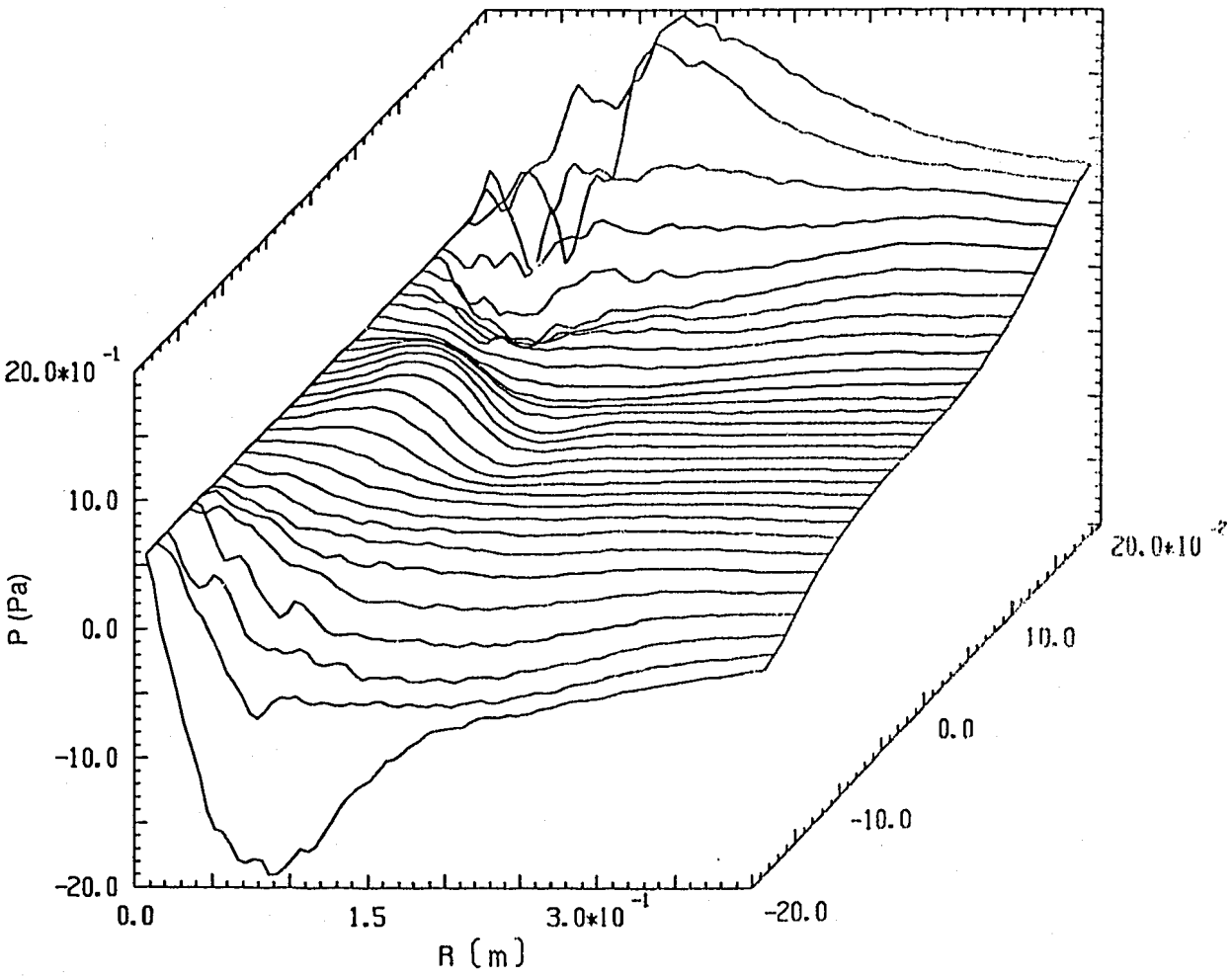

Figure 7

(a)

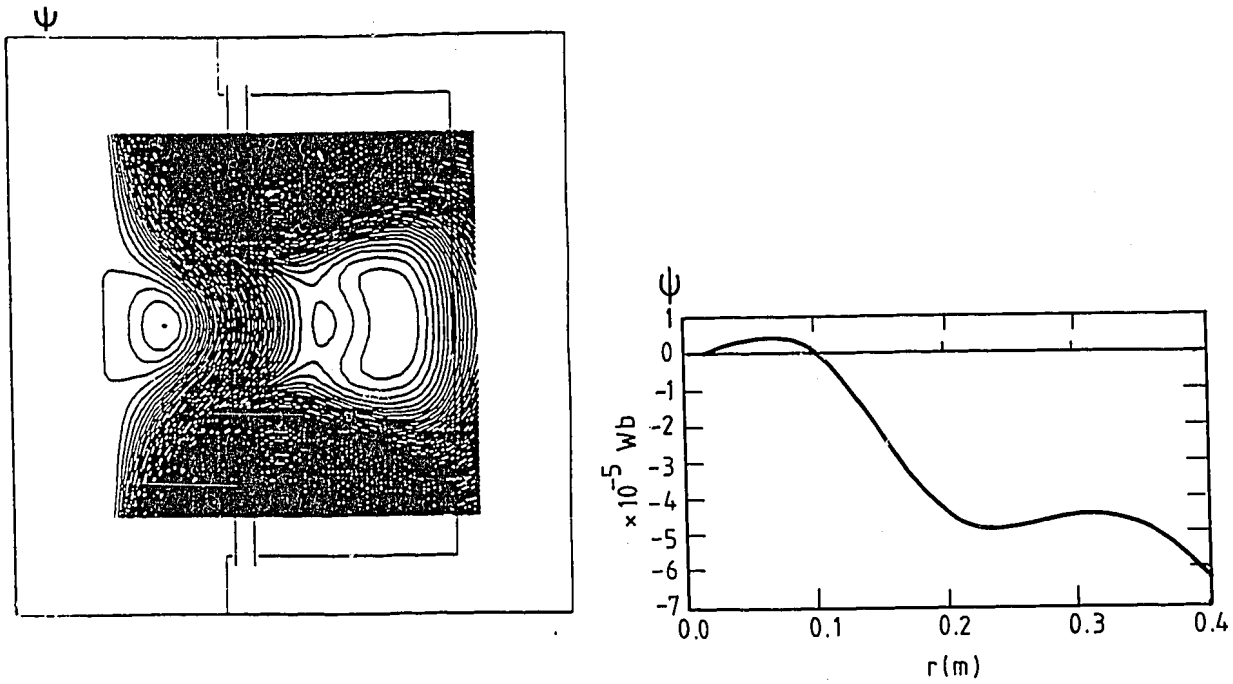

(b)

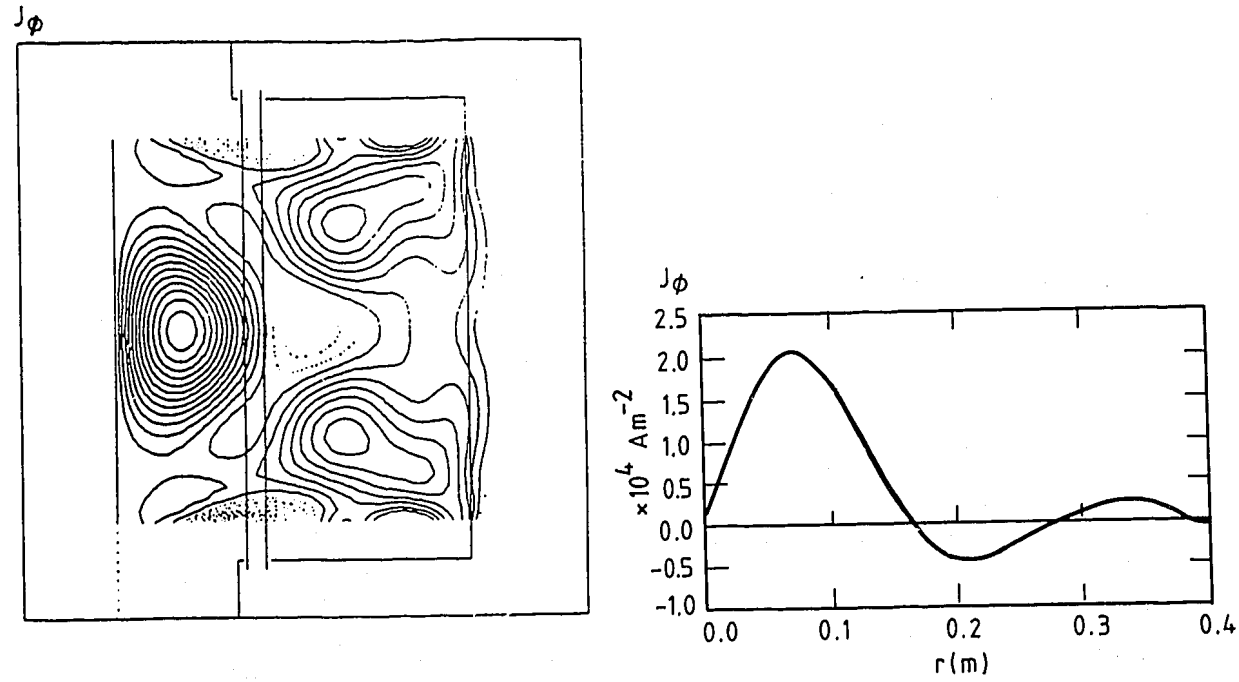

Figure 8 Reproducing **figures 6.27(d)** and **6.32** of Kirolous [1986] showing contour plots and profiles on $z = 0$ of (a) Ψ; (b) J_ϕ; and (c) P. (Continued)

(c)

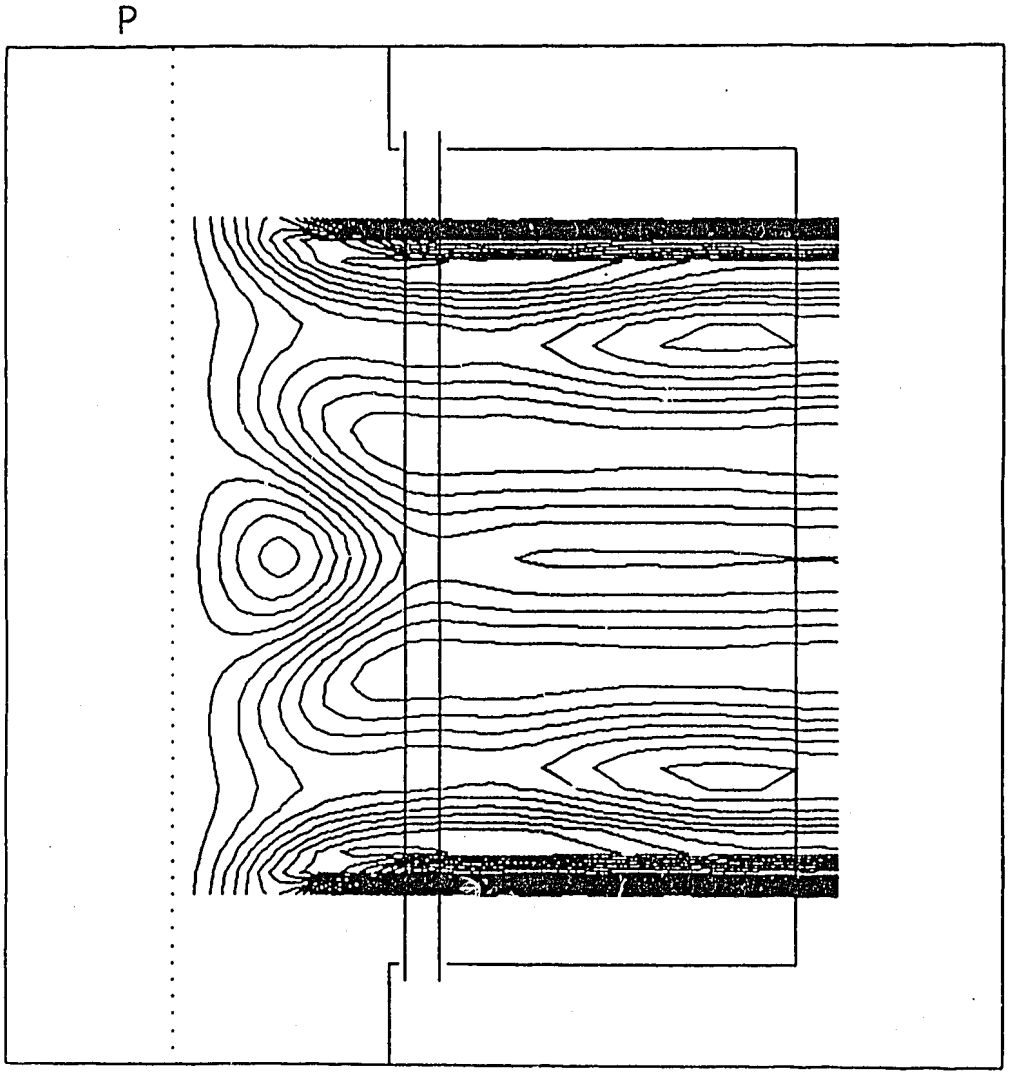

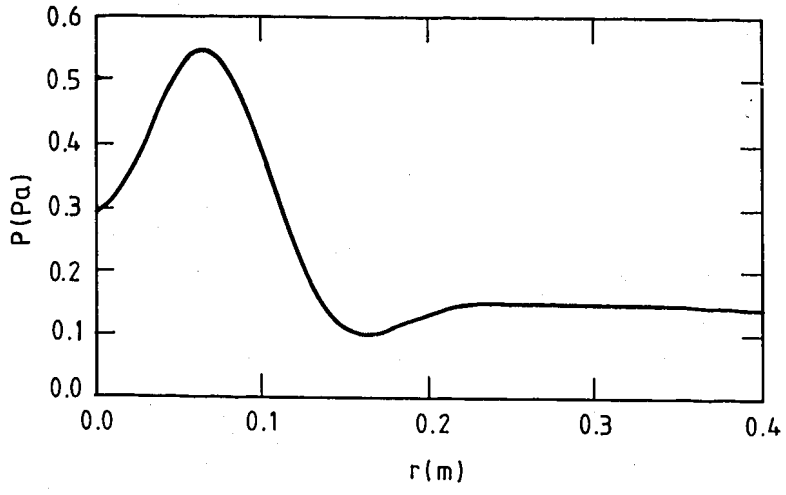

Figure 8